Surface & Coatings Technology xxx (2013) xxx–xxx

Contents lists available at SciVerse ScienceDirect

Surface & Coatings Technology

journal homepage: www.elsevier.com/locate/surfcoat

Improvement in tribological properties of HVOF sprayed WC–Co coatings using electroless Ni–P coated feedstock powders

M. Jafari [a,b,*], M.H. Enayati [a,b], M. Salehi [a,b], S.M. Nahvi [b], C.G. Park [c]

[a] Department of Materials Engineering, Isfahan University of Technology, Isfahan 84156-83111, Iran
[b] Iranian Surface Research and Engineering Centre, Isfahan 84155-337, Iran
[c] Department of Materials Science and Engineering, Pohang University of Science and Technology (POSTECH), Pohang 790-784, Republic of Korea

ARTICLE INFO

Article history:
Received 12 May 2013
Accepted in revised form 25 July 2013
Available online xxxx

Keywords:
WC–Co
HVOF
Friction
Wear behavior

ABSTRACT

The aim of this research is to investigate the sliding friction and wear behavior of a novel WC–Co thermal spray coating deposited from electroless Ni–P coated WC–12Co feedstock powders. The Ni–P coated powders were sprayed on ST37 steel substrate to form a coating, denoted as Ni–P modified WC–12Co coating, using high velocity oxygen fuel (HVOF) process. The X-ray diffractometry (XRD) and high resolution field emission scanning electron microscopy (HR FESEM) were used to analyze microstructural properties of Ni–P coated WC–12Co powders and the resultant coating. The sliding friction and wear behavior of Ni–P modified coating was investigated using a ball-on-disk technique under an applied load of 30 N. The Ni–P modified WC–12Co coating showed extremely lower decarburization level, higher hardness and fracture toughness as compared to the conventional WC–12Co and WC–17Co coatings. The wear rate of Ni–P modified coating was found to be ~3.2×10^{-4} mg/m indicating ~68 and 72% improvement in wear resistance, with respect to the conventional WC–12Co and WC–17Co coatings. Moreover, the Ni–P modified coating exhibited the lowest average friction coefficient of ~0.4 with minor fluctuations. The dominating wear mechanism of Ni–P modified coating was individual WC particles pull-out following extrusion of Ni (Co) binder phase.

1. Introduction

The WC–Co thermal spray coatings are frequently used in wear resistance applications due to their superior mechanical and tribological properties [1–6]. Air plasma spraying (APS), detonation spray coating (DSC) and high velocity oxygen fuel (HVOF) are the most commonly used techniques for deposition of WC–Co coatings. The HVOF process provides advantages over other techniques such as higher velocity and lower temperature of in-flight particles, producing coatings with minimal porosity, excellent adherence to the substrate, larger fraction of retained WC and correspondingly improved wear properties [4,5,7–14]. However, the wear resistance of thermally sprayed WC–Co coatings is always inferior to that of sintered WC–Co hardmetals with identical composition [15,16]. This difference results primarily from decomposition and decarburization of WC during thermal spray leading to the formation of undesirable phases such as W_2C, metallic tungsten, amorphous or nanocrystalline Co–W–C phase and complex carbides in the coating microstructure [3,5,17–19]. It is proposed that during HVOF spray the cobalt matrix melts, upon which WC particles dissolve into the liquid binder enriching the adjacent cobalt matrix in tungsten and carbon. As a result of oxidizing atmosphere of HVOF flame, the carbon dissolved in the binder is oxidized to form CO/CO_2. On impact and subsequent solidification, W_2C phase precipitates from the tungsten-rich binder [1,5,19]. Besides the aforementioned mechanism, direct WC oxidation due to the exposure to the oxidizing HVOF flame is proposed as another mechanism for W_2C formation during HVOF process [19]. The effects of these phase transformations have been reported by many researchers [1,5,20–26] to be deleterious to wear performance of WC–Co coatings. Therefore, many studies have focused on minimizing the extent of decarburization so as to enhance wear properties of thermally sprayed WC–Co coatings. Recently, the effect of using metal clad WC–Co feedstock powders on the microstructural and tribological properties of WC–Co coatings has been investigated by several researchers [2,4,27]. Baik et al. [27] developed a thin Co layer on the surface of WC–Co feedstock powders by immersion into Co-hydrate sol and subsequent hydrogen reduction. They found that the resultant coating exhibits relatively higher wear resistance and lower WC decarburization level, although the W_2C phase was still one of the main constituent in the phase composition of the coating. Saha et al. [2] reported that development of a duplex Co layer around WC–Co powders by chemical vapor deposition (CVD) can prevent significant decarburization of WC during HVOF process, thereby improving the sliding wear resistance of the coatings. Yuan et al. prepared WC–Co–Cu–MoS_2 [28] and WC–Co–Cu–BaF_2/CaF_2 [29] feedstock powders using mechanical milling followed by sinter and crush processes to deposit coatings by APS technique. They observed

* Corresponding author at: Department of Materials Engineering, Isfahan University of Technology, Isfahan 84156-83111, Iran. Tel.: +98 334 2622574; fax: +98 311 3912752.
E-mail address: majid_jafari@ma.iut.ac.ir (M. Jafari).

0257-8972/$ – see front matter © 2013 Elsevier B.V. All rights reserved.
http://dx.doi.org/10.1016/j.surfcoat.2013.07.059

Table 1
Composition of the electroless Ni–P plating bath.

Chemical	Concentration (mlit/lit)
Slotonip 71-1 (basic solution)	160
Slotonip 72 (nickel solution)	70
Slotonip 76 (stabilizer)	7
HF (40 vol.%)	12
Ammonia solution (25 vol.%)	To adjust pH

Table 2
Characteristics of feedstock powders.

Powder	Composition (wt.%) (error: ±1%)						Carbide size (μm)
	W	C	Co	Ni	P	Total binder	
WC–12Co	Balance	5.28	12.1	–	–	12.1	1–6
WC–17Co	Balance	5.18	17.2	–	–	17.2	1–5
Ni–P coated WC–12Co	Balance	5.08	11.7	5.5	0.4	17.6	1–6

significantly low WC decarburization level due to the protection of Cu layer around initial powders. Moreover, they reported superior friction and wear properties for WC–Co–Cu–MoS_2 and WC–Co–Cu–BaF_2/CaF_2 coatings compared to conventional WC–Co ones.

Previous study by the authors [30] showed that WC decarburization during HVOF can be prevented to a large extent by utilizing electroless Ni–P coated WC–12Co powders as feedstock material. In this research, tribological behavior of WC–Co coating deposited from Ni–P coated WC–12Co powders, which is denoted as Ni–P modified WC–12Co coating, is deeply investigated and the changes in the friction and wear properties are explained in terms of the microstructural features of the coating.

2. Experimental procedure

2.1. Materials and methods

Three powders were used as HVOF feedstock material: two commercial WC–12Co and WC–17Co powders from Metallisation Ltd., with spherical morphology and particle size in the range of ~15–45 μm, and an electroless Ni–P coated WC–12Co powder. Electroless Ni–P plating was performed on WC–12Co powders using bath 18071 and Electroless Nickel SLOTONIP 70A process [31] from Schloetter Galvanotechnik. The composition of the electroless plating bath is presented in Table 1.

The bath solution was placed in a glass beaker and heated up to 82 °C using a heater/stirrer. Then, WC–12Co powder particles were added to the bath without any pretreatment. During the plating process, the temperature and pH of the bath were maintained at 80–82 °C and 4.5–5, respectively.

Fig. 1 shows the surface morphology and cross section of Ni–P coated WC–12Co powders.

It is observed that the electroless nickel plating has led to the formation of a thin and uniform Ni–P layer with thickness of ~0.5–1.5 μm around individual WC–12Co powders; moreover, the Ni–P coated powders possess spherical morphology, indicating that the electroless Ni–P layer follows the geometry of initial WC–12Co powders. The characteristics of the feedstock powders are presented in Table 2.

ST37 steel disks with size of Ø30 × 5 mm were used as substrate. Prior to spraying, the disks were grit blasted to obtain mean surface roughness (Ra) of ~15 ± 2 μm, and degreased with acetone. The HVOF spraying was carried out using MET JET III HVOF torch (Metallisation Ltd. at PACO, Isfahan, Iran) with parameters specified in Table 3.

To evaluate the porosity of the coatings, SEM images from coatings cross-section were digitized and analyzed using Clemex microscopy image analysis software. The mean surface roughness (Ra) values of as-sprayed coatings were measured by Taylor-Hobson roughness tester.

2.2. Characterization

The XRD patterns of feedstock powders and resultant coatings were recorded with step size of 0.05 degree per 1 second using a Philips diffractometer (40 kV) with Cu Kα radiation (λ = 0.15406 nm). High resolution FESEM (JEOL JSM-7401F) was used to evaluate the microstructural characteristics of the powders and coatings.

The micro-hardness of the coatings was measured using a Buehler micro-indentation with 2 kg of applied load and dwell time of 20 s. The mean value of 10 indents taken along the mid-plane of the coatings was quoted as the micro-hardness. The indentation fracture toughness of coatings was measured by taking indents on the coatings cross-section at the load of 5 kg. At least 10 indents were performed for each coating. The fracture toughness (K_{IC}) of coatings was calculated using the Eq. (1), assuming that the corner cracks generated from indentations are radial with the Palmqvist geometry [4,5].

$$K_{IC} = 0.0193(H_v d)\left(\frac{E}{H_v}\right)^{\frac{2}{5}}(a)^{-\frac{1}{2}} \quad (1)$$

where H_v and E are Vickers hardness and elastic modulus of the coatings, respectively; a the crack length from indenter corner; and d the

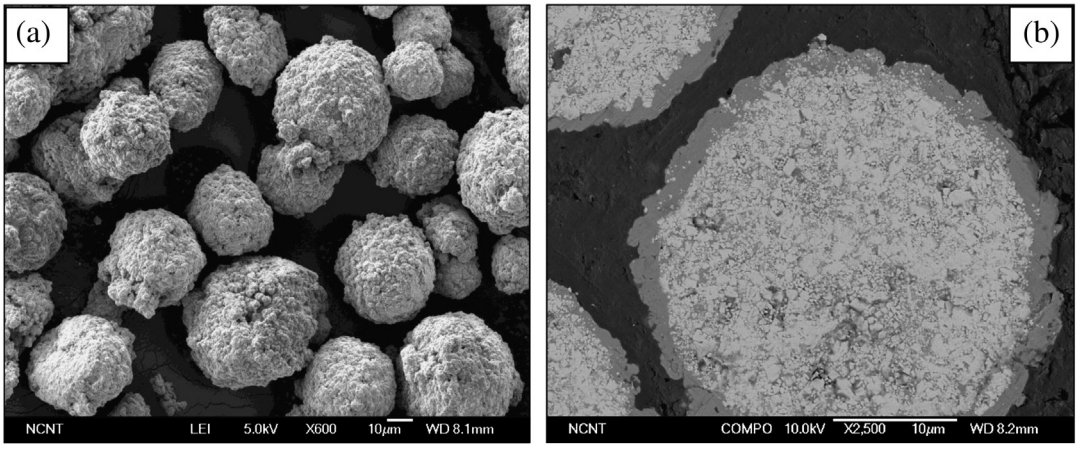

Fig. 1. SEM images of (a) surface morphology and (b) cross-section of Ni–P coated WC–12Co powders.

Table 3
HVOF spray parameters.

Deposition parameter	Value
Spraying distance (mm)	350
Oxygen (mlit/min)	830
Methane (mlit/min)	260
Carrier gas (Nitrogen) (lit/min)	4
Oxygen/fuel ratio	3.19
Powder feed rate (g/min)	40
Spray angle (degree)	90

half-diagonal of the Vickers indentation. The elastic modulus of the coatings was obtained by applying nano-indentations (FIB/Nanoindenter, FEI Company, USA) on the cross-section of the coatings. The elastic modulus values were derived from the initial slope of force-displacement curve during unloading, following the Oliver and Pharr method [32]. Moreover, the SEM images of the indentations were examined to obtain the precise lengths of the corner cracks (a) and the half-diagonal of the Vickers indentation (d).

Friction and wear properties of the coatings were investigated using a ball-on-disk wear test machine. Prior to wear testing, the coatings were ground and polished down to 1 μm resulting in the mean surface roughness values in the range 0.05–0.1 μm. Sintered alumina balls of 7 mm diameter (provided by TIS Wälzkörpertechnologie GmbH, Germany) were employed as counterface. The apparent density and hardness of the balls were 3.95 gr/cm^3 and 70 HRC, respectively. The coatings and balls were ultrasonically cleaned in ethanol for 5 minutes. The tests were conducted at room temperature (25 °C) in air (relative humidity of 28–30%) with sliding speed of 0.1 m/s for 3000 m of sliding distance under vertical load of 30 N. The wear loss was measured from the mass difference of specimens before and after sliding test using an electronic weighing balance of 0.01 mg accuracy. The friction coefficient was continuously recorded with sliding distance. In order to take the repeatability into account, the results for the friction and wear tests were acquired from the average of three readings. To investigate wear mechanism of the coatings, the morphology and elemental analysis of worn surfaces were examined by High resolution FESEM equipped with energy dispersive spectroscopy (EDS).

3. Results and discussion

3.1. Coatings microstructure and properties

The characteristics of WC–12Co, WC–17Co and Ni–P modified WC–12Co coatings are summarized in Table 4.

According to the data given in Table 4, the Ni–P modified coating shows an extremely low porosity percentage of ~0.3%, while higher porosity levels of 1.6 and 1.3% were measured in the case of conventional WC–12Co and WC–17Co coatings, deposited under the same spray conditions. This suggests that a denser coating with improved inter-splat cohesion can be obtained using Ni–P coated WC–12Co as feedstock powder.

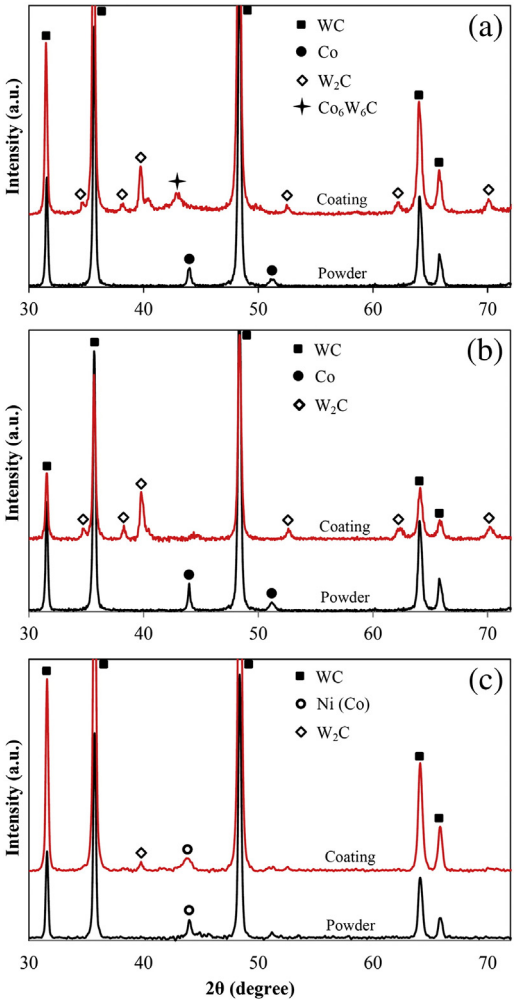

Fig. 2. XRD patterns of powders and coatings of (a) WC–12Co, (b) WC–17Co and (c) Ni–P modified WC–12Co.

Fig. 2 demonstrates the XRD patterns of WC–12Co, WC–17Co and Ni–P coated WC–12Co powders and the corresponding coatings.

The XRD patterns of WC–12Co and WC–17Co powders show that they contain WC and Co phases. Similarly, the peaks corresponding to WC and Ni (Co) phases can be observed on XRD spectrum of Ni–P coated WC–12Co powder. The XRD pattern of WC–12Co coating confirms the presence of W_2C and η (Co_6W_6C) phases, while no free cobalt peak was detected suggesting that cobalt has reacted with carbon and tungsten to form η (Co_6W_6C) phase. The W_2C peaks are also observed on the XRD pattern of WC–17Co coating. Therefore, it can be concluded that the WC phase is significantly decomposed and decarburized during HVOF process of conventional WC–12Co and WC–17Co coatings. The XRD pattern of Ni–P modified coating, however, reveals WC and Ni (Co) peaks as the main constituents along with a very small W_2C peak; furthermore, no η phase is observed on the XRD pattern. This phase composition proves that negligible WC decarburization has occurred in

Table 4
Comparison between the characteristics of WC–12Co, WC–17Co and Ni–P modified WC–12Co coatings.

Coating	Porosity (%)	Thickness (μm)	R_a (μm)	Micro-hardness (H_v)	E (GPa)	K_{IC} (MPa m$^{1/2}$)
WC–12Co	1.6 ± 0.5	417 ± 25	5.6 ± 0.6	1120 ± 54	300 ± 1.7	5.76 ± 1.24
WC–17Co	1.3 ± 0.6	432 ± 33	5.4 ± 0.5	1080 ± 42	298 ± 2.0	6.12 ± 1.48
Ni–P modified WC–12Co	0.3 ± 0.1	420 ± 15	5.1 ± 0.3	1168 ± 19	302 ± 1.3	9.86 ± 0.70

Please cite this article as: M. Jafari, et al., Surf. Coat. Technol. (2013), http://dx.doi.org/10.1016/j.surfcoat.2013.07.059

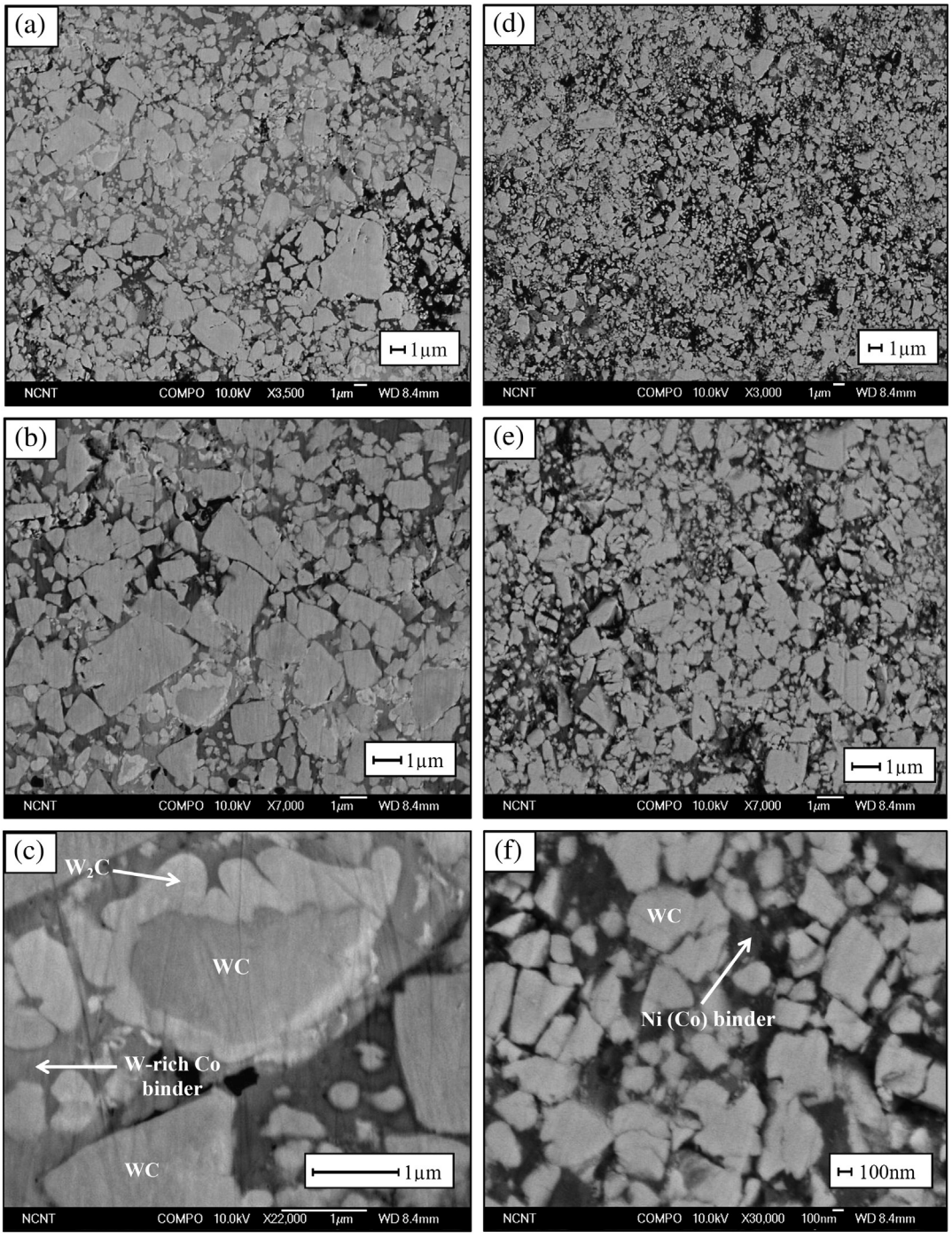

Fig. 3. BSE images of WC–12Co (a–c) and Ni–P modified (d–f) coatings microstructure at different magnifications.

the case of Ni–P modified coating during HVOF process. A quantitative analysis on the extent of WC decarburization of the coatings is presented in the previous study [30]. Comparing the carbon content of initial powders and resultant coatings verified insignificant decarburization level of 2.6% in the case of Ni–P modified WC–12Co coating, while substantially higher decarburization values of 16.3 and 17.6% were found for conventional WC–12Co and WC–17Co coatings, respectively [30].

The back-scattered electron (BSE) images from microstructure of WC–12Co and Ni–P modified coatings are illustrated in Fig. 3.

As shown in Fig. 3 (a–c), the evidences of WC decarburization can be observed in some regions of WC–12Co coating microstructure. These regions are characterized by brighter contrast, representing the tungsten-rich cobalt matrix, in which carbide particles with rounded morphology are located. As well, some carbides are surrounded by an irregular bright fringe which is identified as W_2C phase [19,33]. Similar microstructure was observed for WC–17Co coating.

In contrast, the BSE images of Ni–P modified WC–12Co coating reveal more homogenous microstructure in which blocky WC particles are distributed within the dark matrix (Fig. 3d–f). This feature can also be observed in the case of very small carbide particles (Fig. 3f), which are well-known to be more susceptible to decarburization

Please cite this article as: M. Jafari, et al., Surf. Coat. Technol. (2013), http://dx.doi.org/10.1016/j.surfcoat.2013.07.059

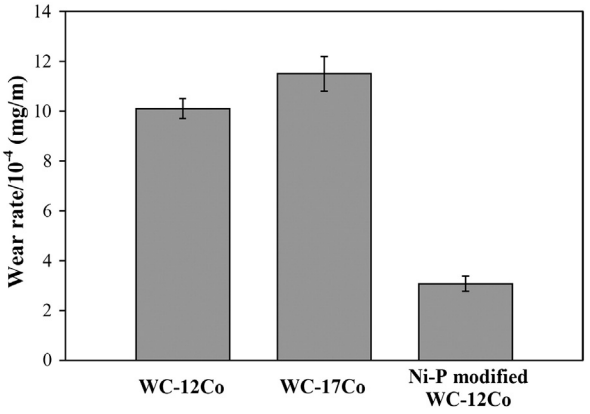

Fig. 4. Sliding wear rates of WC–12Co, WC–17Co and Ni–P modified WC–12Co coatings.

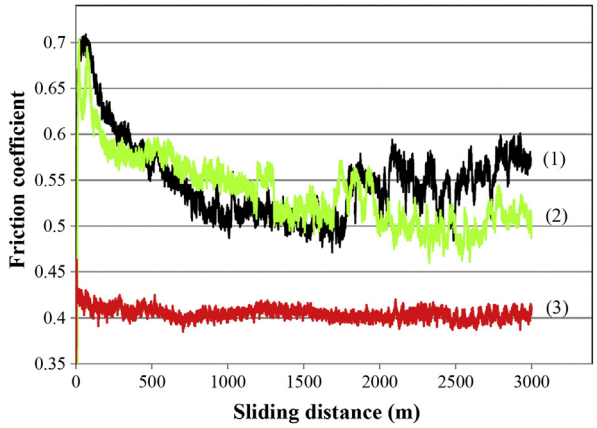

Fig. 5. Plot of friction coefficient versus sliding distance for (1) WC–12Co, (2) WC–17Co and (3) Ni–P modified WC–12Co coatings.

[34–37]. Therefore, the Ni–P modified WC–12Co coating experienced no significant decarburization during HVOF in agreement with the XRD results. It is suggested that the Ni–P outer layer melts during HVOF process and absorbs latent heat of fusion, decreasing the heating degree of inner WC–Co particles. This causes less WC dissolution into the cobalt matrix and consequently lower degree of decarburization. Moreover, the Ni–P layer around the WC–12Co powders reduces the WC exposure to oxidizing flame, preventing direct WC oxidation and thereby W_2C formation during HVOF process.

Mechanical properties of the coatings are summarized in Table 4. The Ni–P modified coating shows the hardness of ~1168 H_v, indicating higher value compared to the conventional WC–12Co and WC–17Co coatings with hardness of 1120 and 1080 H_v, respectively. The higher hardness of Ni–P modified coating can be explained by its low porosity, high inter-splat cohesion and high WC retention within the coating microstructure [34,38]. The indentation fracture toughness calculated for the coatings reveals a maximum value of 9.86 MPa $m^{1/2}$ for Ni–P modified coating, indicating 71.2 and 61.1% increase with respect to the WC–12Co and WC–17Co coatings.

3.2. Sliding wear behavior

The wear rates of WC–12Co, WC–17Co and Ni–P modified WC–12Co coatings worn under a constant load of 30 N are shown in Fig. 4.

The wear rates of WC–12Co and WC–17Co coatings were 10.1×10^{-4} and 11.5×10^{-4} mg/m, while the Ni–P modified coating exhibits significantly lower wear rate of ~3.2×10^{-4} mg/m. This represents approximately 68 and 72% improvement in wear resistance in comparison with the conventional WC–12Co and WC–17Co coatings, respectively. Fig. 5 demonstrates the variation of friction coefficient as a function of sliding distance for the coatings.

The friction coefficient of WC–12Co coating shows an initial increase to a value of 0.7 due to the static friction force [39]. This is followed by a continuous decrease to a wide region in which the friction coefficient varies in the range of ~0.5–0.6 with significant oscillations. The friction coefficient of WC–17Co coating varies in a relatively similar manner to the WC–12Co coating but indicates slightly lower variation range of ~0.45–0.55. On the other hand, the Ni–P modified WC–12Co coating exhibits the lowest friction coefficient of ~0.4 with negligible fluctuations compared to the conventional coatings tested under the same conditions.

To evaluate the abovementioned friction and wear behavior, the worn surface of the coatings was examined by SEM-EDS. Fig. 6 shows SEM images from worn surface of WC–12Co coating at different magnifications.

Fig. 6a shows the evidences of severe cracking, delamination and pitting in the worn surface of WC–12Co coating which result in the large amounts of material loss from the wear track and therefore high wear rate (see Fig. 4). Higher magnification image (Fig. 6b) proves the extensive sub-surface cracking, with cracks propagating parallel to the worn surface. Besides, a shallow ploughing mode of wear can be observed as evidenced by the slim grooves on the worn surface. The BSE image from worn surface of WC–12Co coating (Fig. 6c) reveals that a tribo-reaction layer with a relatively dark contrast has been formed on the wear track during wear test. The EDS analysis (Fig. 6d) verifies the presence of tungsten, cobalt, aluminum, carbon and oxygen in the composition of the tribo-reaction layer, indicating that this layer is formed by mixing the materials removed from the cermet coating and alumina ball. It seems that the alternating formation and delamination of the tribo-reaction layer occurred during wear test, changes the load applying on the sample by changing the area of surface contact between the sample and alumina ball [40]. This causes significant oscillations observed in the friction coefficient profile of conventional WC–12Co coating, as shown in Fig. 5.

The SEM images from worn surface of WC–17Co coating are shown in Fig. 7.

It is observed that significant loss of materials from the wear track of WC–17Co coating has occurred due to the severe delamination and pitting during wear test, signifying almost similar wear mechanism to WC–12Co coating.

In general, during the sliding wear test, the cermet coatings are exposed to repeated compressive and tensile loadings due to the rotation of alumina ball. This can result in the crack initiation in the sub-surface where the maximum shear stress exists [28,41,42]. In the case of conventional coatings, which have undergone greater levels of decarburization, the cracks propagate mainly along the brittle regions of microstructure such as W_2C and tungsten-rich binder phases [21,28,43], leading to the formation of a network of sub-surface cracks. As the time progresses, large-scale materials removal occurs from discrete areas of wear track. Therefore, one can conclude that sub-surface cracking induced delamination is the predominant wear mechanism for the conventional WC–12Co and WC–17Co coatings.

The SEM images from worn surface of Ni–P modified coating are shown in Fig. 8.

The wear track of Ni–P modified WC–12Co coating exhibits a relatively smooth surface in which no significant evidence of sub-surface cracking can be observed. This may arise from the higher fracture toughness obtained for Ni–P modified coating which causes higher resistance against crack propagation in comparison with the conventional coatings. As discussed previously, high level of retained

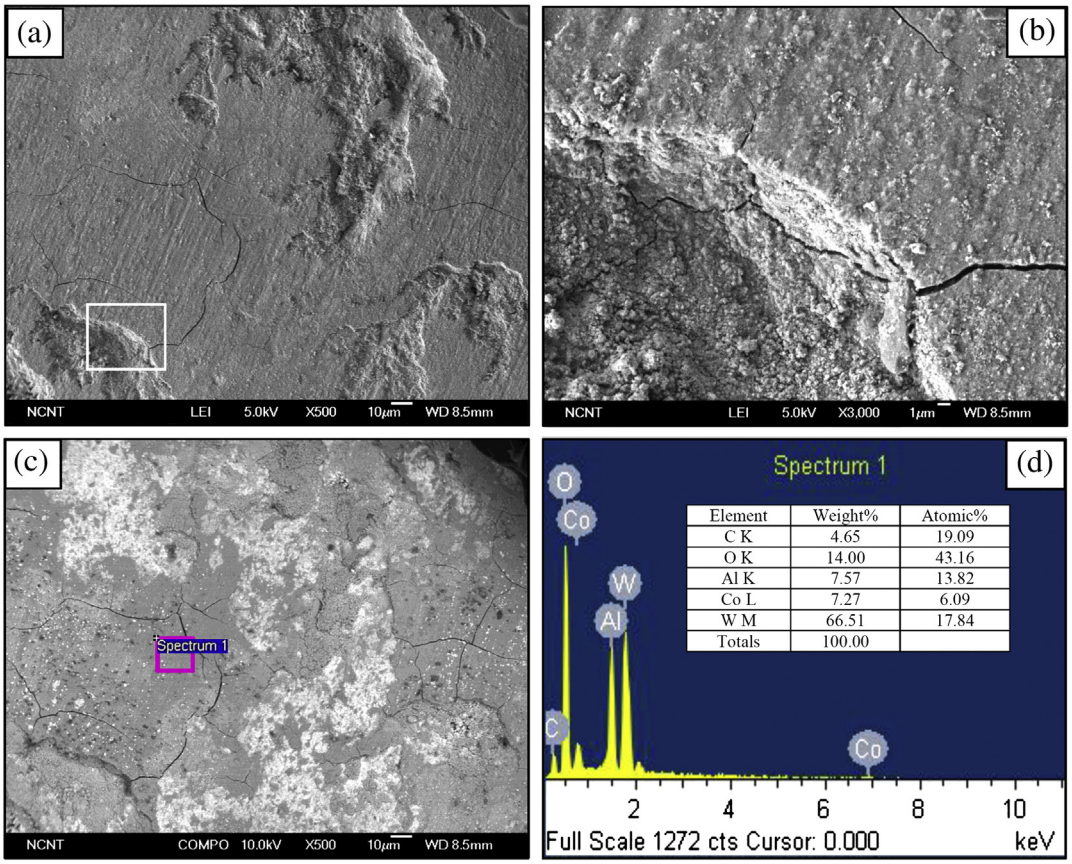

Fig. 6. (a,b) SEM images from worn surface of WC–12Co coating at different magnifications, (c) BSE image from worn surface of WC–12Co coating and (d) EDS analysis from wear track.

WC particles within the Ni (Co) matrix was obtained in the microstructure of Ni–P modified coating. During sliding wear test, the soft and ductile Ni (Co) matrix, which is more prone to plastic deformation, forms a thin layer at sliding interface in which the carbides are embedded with relatively strong bonding (see Fig. 8b); therefore, carbide particles are supported by metallic matrix to perform their wear resistance function against alumina ball, resulting in the substantial decrease in the sliding wear rate, as shown in Fig. 4. In addition, presence of the Ni (Co) layer containing WC particles on the wear the wear track effectively reduces the actual area of surface contact between the coating and alumina counterface by acting as a lubricant [17], causing the lower friction coefficient with insignificant oscillation. This is also confirmed by EDS analysis that shows extremely low Al content in the worn surface of Ni–P modified coating, denoting small amount of materials transfer from alumina ball to the wear track.

As the test continues, some parts of the Ni (Co) matrix are abraded by the compressive stress of alumina ball. This is followed by loss of carbide particles from the areas where the support of the metallic matrix is not present. Therefore, wear mechanism of Ni–P modified coating can be characterized by individual WC particles pull-out following the extrusion of metallic matrix. This wear mechanism is also proposed by other

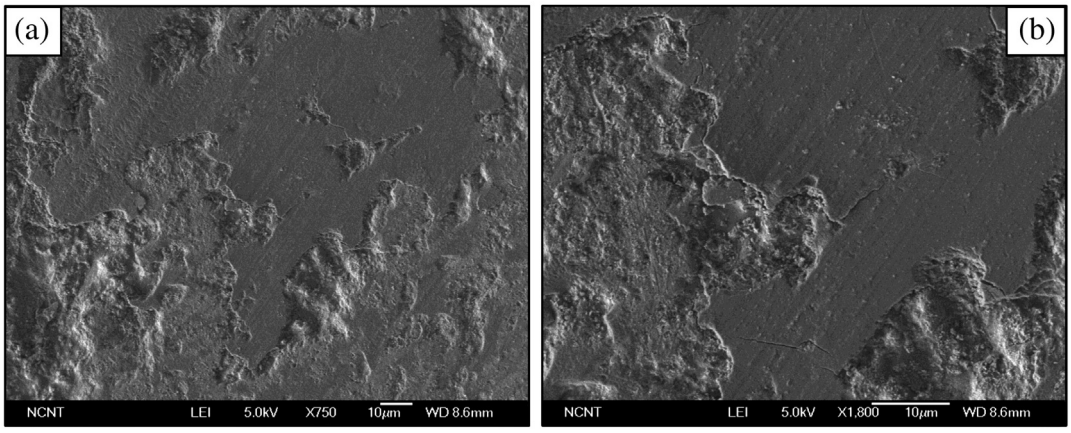

Fig. 7. (a,b) SEM images from worn surface of WC–12Co coating at different magnifications.

Please cite this article as: M. Jafari, et al., Surf. Coat. Technol. (2013), http://dx.doi.org/10.1016/j.surfcoat.2013.07.059

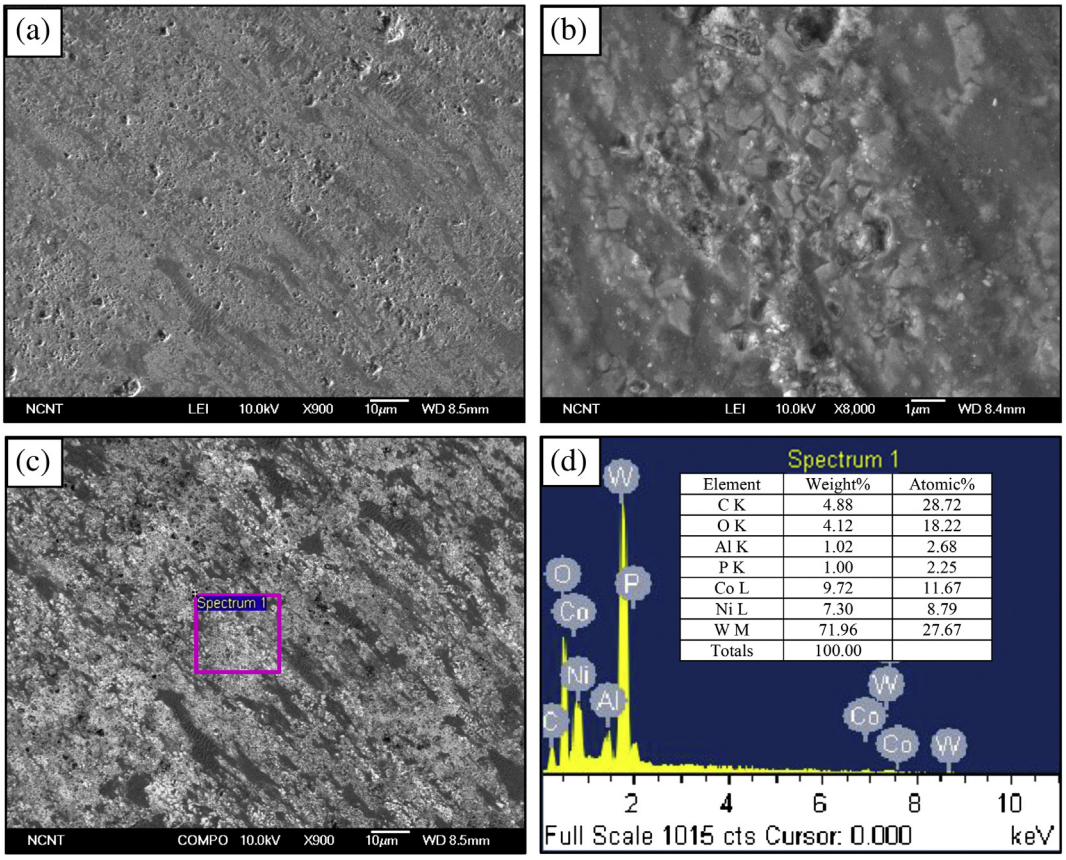

Fig. 8. (a,b) SEM images from worn surface of Ni–P modified coating at different magnifications, (c) BSE image from worn surface of Ni–P modified WC–12Co coating and (d) EDS analysis from wear track.

researchers in the case of sintered WC–Co hardmetal [43] and WC–Co based thermal spray coatings with low decarburization level [15,17,44], which have suffered from less damage during wear experiment.

Finally, it can be concluded that significantly improved tribological performance in terms of sliding friction and wear behavior can be obtained for WC–Co coatings by utilizing electroless Ni–P coated WC–Co powders as HVOF feedstock material.

4. Conclusions

This research was aimed at evaluating the sliding friction and wear behavior of a novel WC–Co coating deposited from electroless Ni–P coated WC–12Co powders. The following conclusions are drawn:

- The Ni–P modified WC–12Co coating showed extremely lower decarburization level, higher hardness and fracture toughness in comparison with the conventional WC–12Co and WC–17Co coatings.
- The wear rate of Ni–P modified coating was ~3.2×10^{-4} mg/m indicating approximately 68 and 72% improvement in wear resistance, with respect to the conventional WC–12Co and WC–17Co coatings.
- The lowest friction coefficient of ~0.4 with negligible fluctuations was found in the case of Ni–P modified WC–12Co coating, representing much lower value than that of WC–12Co and WC–17Co coatings.
- The dominating wear mechanism for conventional WC–12Co and WC–17Co coatings was sub-surface cracking induced delamination, while it was proposed that the Ni (Co) binder phase extrusion followed by carbide particles pull-out is the predominant wear mechanism Ni–P modified coating.

References

[1] N.S. Lim, S. Das, S.Y. Park, M.C. Kim, C.G. Park, Surf. Coat. Technol. 205 (2010) 430–435.
[2] G.C. Saha, T.I. Khan, Metall. Mater. Trans. A 41A (2010) 3000–3009.
[3] P. Chivavibul, M. Watanabe, S. Kuroda, J. Kawakita, M. Komatsu, K. Sato, J. Kitamura, J. Therm. Spray Technol. 20 (5) (2011) 1098–1109.
[4] A. Mateen, G.C. Saha, T.I. Khan, F.A. Khalid, Surf. Coat. Technol. 206 (2011) 1077–1084.
[5] P. Chivavibul, M. Watanabe, S. Kuroda, K. Shinoda, Surf. Coat. Technol. 202 (2007) 509–521.
[6] P. Suresh Babu, B. Basu, G. Sundararajan, Acta Mater. 56 (2008) 5012–5026.
[7] T. Sudaprasert, P.H. Shipway, D.G. McCartney, Wear 255 (2003) 943–949.
[8] R.W. Smith, R. Knight, J. Met. 47 (1995) 32–39.
[9] V.V. Sobolev, J.M. Guilemany, Int. Mater. Rev. 41 (1996) 13–31.
[10] M. Li, P.D. Christofides, Chem. Eng. Sci. 61 (2006) 6540–6552.
[11] B.R. Marple, R.S. Lima, J. Therm. Spray Technol. 14 (2005) 67–76.
[12] Z.G. Ban, L.L. Shaw, J. Therm. Spray Technol. 12 (1) (2003) 112–119.
[13] H.L. De Villiers Lovelock, J. Therm. Spray Technol. 7 (3) (1998) 357–373.
[14] J.R. Fincke, W.D. Swank, D.C. Haggard, in: C.C. Berndt, S. Sampath (Eds.), Comparison of the characteristics of HVOF and plasma thermal spray in thermal spray industrial applications, ASM International, Materials Park, OH, 1994, pp. 325–330.
[15] P. Suresh Babu, B. Basu, G. Sundararajan, Wear 268 (2010) 1387–1399.
[16] S.F. Wayne, S. Sampath, J. Therm. Spray Technol. 1 (1992) 307–316.
[17] Q. Yang, T. Senda, A. Ohmori, Wear 254 (2003) 23–34.
[18] V.V. Sobolev, J.M. Guilemany, J. Nutting, High Velocity Oxy-Fuel Spraying: Theory, Structure–Property Relationships And Applications, Maney Publishing, UK, 2004.
[19] J.M. Guilemany, J.M. de Paco, J. Nutting, J.R. Miguel, Metall. Mater. Trans. A 30A (1999) 1913–1921.
[20] R.J.K. Wood, Int. J. Refract. Met. Hard Mater. 28 (2010) 82–94.
[21] D.A. Stewart, P.H. Shipway, D.G. McCartney, Wear 789 (1999) 225–229.
[22] S. Usmani, S. Sampath, D.L. Houck, D. Lee, Tribol. Trans. 40 (3) (1997) 470–478.
[23] C. Verdon, A. Karimi, J.L. Martin, Mater. Sci. Eng. A 246 (1–2) (1998) 11–24.
[24] Y. Ishikawa, J. Kawakita, S. Sawa, T. Itsukaichi, Y. Sakamoto, M. Takaya, S. Kuroda, J. Therm. Spray Technol. 14 (3) (2005) 384–390.
[25] M. Watanabe, A. Owada, S. Kuroda, Y. Gotoh, Surf. Coat. Technol. 201 (3–4) (2006) 619–627.
[26] Y. Ishikawa, S. Kuroda, J. Kawakita, Y. Sakamoto, M. Takaya, Surf. Coat. Technol. 201 (8) (2007) 4718–4727.
[27] K.H. Baik, J.H. Kim, B.G. Seong, Mater. Sci. Eng., A 449–451 (2007) 846–849.

Please cite this article as: M. Jafari, et al., Surf. Coat. Technol. (2013), http://dx.doi.org/10.1016/j.surfcoat.2013.07.059

[28] J. Yuan, Y. Zhu, X. Zheng, H. Ji, T. Yang, J. Alloy Compd. 509 (2011) 2576–2581.
[29] J. Yuan, Y. Zhu, H. Ji, X. Zheng, Q. Ruan, Y. Niu, Z. Liu, Y. Zeng, Appl. Surf. Sci. 256 (2010) 4938–4944.
[30] M. Jafari, M.H. Enayati, M. Salehi, S.M. Nahvi, C.G. Park, Mater. Sci. Eng., A 578 (2013) 46–53.
[31] www.schloetter.de/en/processes/18-electroless-nickel.
[32] W.C. Oliver, G.M. Pharr, J. Mater. Res. 7 (1992) 1564–1583.
[33] D.A. Stewart, P.H. Shipway, D.G. McCartney, Surf. Coat. Technol. 105 (1998) 13–24.
[34] J. He, M. Ice, S. Dallek, E.J. Lavernia, Metall. Mater. Trans. A 31A (2000) 541–553.
[35] B.H. Kear, G. Skandan, R.K. Sadangi, Scripta Mater. 44 (2001) 1703–1707.
[36] D.A. Stewart, P.H. Shipway, D.G. McCartney, Acta Mater. 48 (2000) 1593–1604.
[37] J.M. Guilemany, S. Dosta, J. Nin, R. Miguel, J. Therm. Spray Technol. 14 (2005) 405–413.
[38] C.J. Li, A. Ohmori, Y. Harada, J. Mater. Sci. 31 (1996) 785–794.
[39] E. Celik, O. Culha, B. Uyulgan, N.F. Ak Azem, I. Ozdemir, A. Turk, Surf. Coat. Technol. 200 (2006) 4320–4328.
[40] E. Sanchez, E. Bannier, M.D. Salvador, V. Bonache, J.C. Garcia, J. Morgiel, J. Grzonka, J. Therm. Spray Technol. 19 (5) (2010) 964–974.
[41] J. Yuan, Y. Zhu, X. Zheng, Q. Ruan, H. Ji, Appl. Surf. Sci. 255 (2009) 7959–7965.
[42] L. Du, B. Xu, S. Dong, W. Zhang, J. Zhang, H. Yang, H. Wang, Surf. Coat. Technol. 202 (2008) 3709–3714.
[43] P.H. Shipway, D.G. McCartney, T. Sudaprasert, Wear 259 (2005) 820–827.
[44] S.L. Liu, X.P. Zheng, G.Q. Geng, Wear 269 (2010) 362–367.

Please cite this article as: M. Jafari, et al., Surf. Coat. Technol. (2013), http://dx.doi.org/10.1016/j.surfcoat.2013.07.059